ADVANCED FUNCTIONAL MATERIALS
www.afm-journal.de

Systematic Doping Control of CVD Graphene Transistors with Functionalized Aromatic Self-Assembled Monolayers

Nathan Cernetic, Sanfeng Wu, Joshua A. Davies, Benjamin W. Krueger, Daniel O. Hutchins, Xiaodong Xu, Hong Ma, and Alex K.-Y. Jen**

Recent reports have shown that self-assembled monolayers (SAMs) can induce doping effects in graphene transistors. However, a lack of understanding persists surrounding the quantitative relationship between SAM molecular design and its effects on graphene. In order to facilitate the fabrication of next-generation graphene-based devices it is important to reliably and predictably control the properties of graphene without negatively impacting its intrinsic high performance. In this study, SAMs with varying dipole magnitudes/directions are utilized and these values are directly correlated to changes in performance seen in graphene transistors. It is found that, by knowing the z-component of the SAM dipole, one can reliably predict the shift in graphene charge neutrality point after taking into account the influence of the metal electrodes (which also play a role in doping graphene). This relationship is verified through density functional theory and comprehensive device studies utilizing atomic force microscopy, X-ray photoelectron spectroscopy, Raman spectroscopy, and electrical characterization of graphene transistors. It is shown that properties of graphene transistors can be predictably controlled with SAMs when considering the total doping environment. Additionally, it is found that methylthio-terminated SAMs strongly interact with graphene allowing for a cleaner graphene transfer and enhanced charge mobility.

1. Introduction

Graphene is a two-dimensional semimetal with promising electrical and optical properties that consists of sp^2-hybridized carbon atoms arranged in a honeycomb lattice. The electronic properties arising from the unique crystal structure of graphene result in a linear dispersion for low energy carriers, which can be described as zero rest-mass relativistic particles with exemplary transport properties.[1–3] Electron mobility as high as 200 000 $cm^2\ V^{-1}\ s^{-1}$ can be achieved once extrinsic factors such as scattering centers from underlying substrates, adsorbates, and defects within graphene itself are controlled.[4–9] In order to utilize graphene for next generation electronic devices it is necessary to have precise control of carrier concentration and polarity without disrupting its intrinsic properties. Carrier doping of graphene has so far been achieved via chemical doping,[10–13] substitutional doping,[14–16] electric field modulation,[17,18] and metal contact doping.[19,20]

Recent reports have also shown it is possible to modulate the properties of graphene by modifying the underlying dielectric surface with a self-assembled monolayer (SAM) resulting in doping control without compromising the intrinsic graphene performance.[21–24] However, these studies use exfoliated graphene rather than the more commercially viable CVD-based graphene. In addition, exfoliation severely limits the ability to do a systematic and statistical study based on multiple devices due to the taxing processing steps necessary to fabricate individual devices. In order to circumvent this issue, characterization of these devices is mainly attributed to multiple Raman scans on a few pieces of modified graphene rather than multiple pieces of graphene. While such methodology is useful for obtaining an overall picture of the graphene doping environment it makes it difficult to understand the exact relationship between SAMs and graphene. SAMs are commonly used in organic field-effect transistors to modify the work function of metal electrodes,[25,26] quench charge trap sites at the interface between semiconductor and metal or dielectric,[27–29] and modulate the position of the threshold voltage.[30–32] SAMs represent an ideal platform for control of graphene electronics as they can be designed and functionalized at the molecular scale to cater to specific device requirements. However, there is still a need for better understanding of how SAM-treated dielectrics modulate the doping of graphene devices. In particular, an understanding of how the SAM dipole, while taking into account metal electrode effects, influences graphene has yet to be studied. In this paper we

N. Cernetic, J. A. Davies, D. O. Hutchins, Prof. H. Ma, Prof. A. K.-Y. Jen
Department of Materials Science and Engineering
Box 352120
University of Washington
Seattle, WA 98195–2120, USA
E-mail: hma@u.washington.edu; ajen@u.washington.edu
S. Wu, B. W. Krueger, Prof. X. Xu
Department of Physics, Box 351560
University of Washington
Seattle, WA 98195–1560, USA
Prof. A. K.-Y. Jen
Department of Chemistry, Box 351700
University of Washington
Seattle, WA 98195–1700, USA

DOI: 10.1002/adfm.201303952

© 2014 WILEY-VCH Verlag GmbH & Co. KGaA, Weinheim

demonstrate that SAMs can be used to reliably and predictably control the charge carrier concentration of graphene transistors without negatively impacting charge carrier mobility while taking into account the total doping environment.

2. Results and Discussion

SAMs were grown via immersion assembly on cleaned 300 nm thick SiO_2 with an AlO_x adhesion layer between the SAM and dielectric. Due to the weak interaction between the phosphonic acid SAM binding group and silanol (Si–OH) on the SiO_2 oxide surface, an AlO_x adhesion layer was necessary in order to form a covalent bond between the SAM and dielectric.[33] Functionalized aromatic SAMs of (4-cyanophenyl)phosphonic acid, 4-(trifluoromethyl)phenylphosphonic acid, phenylphosphonic acid, 4-(methylthio)phenyl phosphonic acid, and 4-(methoxy) phenylphosphonic acid were used to systematically study the influence of SAM dipoles on CVD graphene transistors. These SAMs will be referred to throughout this paper as CN, CF_3, Ph, MeS, and MeO respectively and can be seen in **Figure 1**a.

Phosphonic acid molecules were used to functionalize the AlO_x/SiO_2 dielectric layer due to advantages over traditional silane based SAMs such as: high thermal stability,[34] binding not limited by surface hydroxyl content,[35] and no homocondensation.[36] These factors, in conjunction with the chosen molecular designs, result in the formation of densely packed SAMs with high thermal stability and similar packing density. Atomic force microscopy (AFM) and water contact angle goniometry were used to characterize each SAM assembled on AlO_x/SiO_2 surface. All SAMs show a similar smooth morphology with an RMS roughness between 0.2 and 0.3 nm, which is comparable to the untreated dielectric surface. A representative image of the SAM topography can be seen in Figure 1b.

The static water contact angle for each SAM on the AlO_x dielectric was determined to be 57°, 75°, 61°, 68°, and 64° for CN, CF_3, Ph, MeS, and MeO, respectively. For reference, the water contact angle for the untreated dielectric surface is less than 10°. The standard deviation of contact angle for each SAM is less than 3°, indicating uniform and continuous coverage across the entire dielectric surface. The low RMS roughness and preserved contact angle after extensive sonication in organic solvents post-assembly, indicates the formation of a dense and homogenous molecular monolayer that is chemically bound to the dielectric surface and free of physisorbed aggregate.

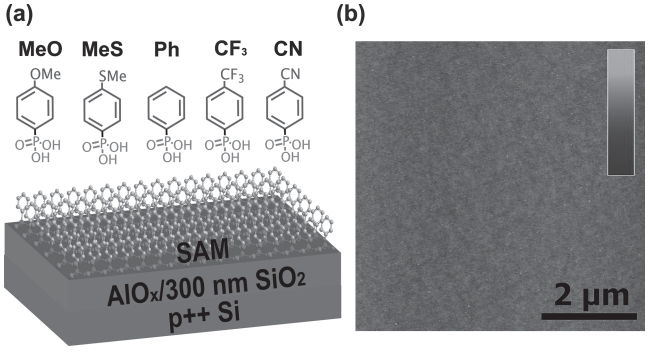

Figure 1. a) Chemical structure of each SAM used in this study with assembled SAM schematic and b) representative topology measured by AFM of assembled SAM on AlO_x/SiO_2 dielectric. The z-scale for the AFM image shown in the top right is 0–5 nm.

DFT calculations were used to extract the molecular dipole of the SAMs[37] from geometry-optimized structures of single molecules. DFT[38,39] geometry optimizations were performed using Gaussian 09(A.02)[40] employing the Perdew, Burke, and Ernzhof[41] functional (PBE) with the split valence basis set (SVP) from Schaefer, Horn, and Ahlrichs[42] and the SVPFit auxiliary basis.[43] Molecules were rotated into frame so to define the longest molecular axis as the *z* direction; that is, the vector from the phosphorous to the para-standing carbon of the phenyl SAMs. Frequency calculations and population analysis were performed on the optimized geometries and minima were verified through normal mode analyses. Finally, conformational analysis was performed on all molecules to determine the lowest energy conformations. A summarization of calculated dipoles along the z-axis can be found in **Table 1**.

A Renishaw inVia Raman Microscope with 514 nm laser was used to determine the quality of graphene on SAM modified dielectric surface via the characteristic phonon peaks of graphene. **Figure 2** shows a representative Raman spectrum of graphene on the SAM/dielectric. The lack of a D peak (≈1350 cm^{-1}) implies high quality, defect free graphene.[44] The 2D peak (≈2685 cm^{-1}) is spectrally sharp and its intensity is about four times greater than that of the G peak (≈1585 cm^{-1}), which are characteristics of monolayer graphene.[45–47]

To obtain a better understanding of the effect a given SAM-dipole has on the electronic properties of graphene, X-ray photoelectron spectroscopy (XPS) was used to determine the work function as well as the characteristic C1s binding energy peak of graphene on the various SAM-treated AlO_x/SiO_2 surfaces. In order to minimize the influence of extrinsic factors such as atmospheric adsorbants, substrates were annealed under an inert atmosphere of N_2 at 200 °C for 2 h and were only exposed to ambient conditions for a few seconds while transferring into the XPS system. A –5 V bias was applied to the graphene/SAM substrate relative to the spectrometer, and the location of the secondary electron cut-off energy was determined at a take-off angle of 90° via linear extrapolation with respect to the background baseline as described elsewhere.[48] Graphene on an AlO_x/SiO_2 dielectric without SAM treatment was determined to have a work function of 4.31 ± 0.02 eV which is comparable to that in literature for CVD grown graphene.[49] The relative work function shift of graphene on SAM-treated dielectric surfaces was within a range of 0.5 eV dependent on the SAM dipole direction and magnitude. A linear relationship, with the exception of MeS, between the SAM dipole and the average shift in graphene work function is shown in **Figure 3**a.

The surface dipole generated by the SAM is expected to affect the work function of graphene based on the following relationship:[50,51]

$$\Delta\Phi_{SAM} = \left(\frac{eN\mu_z}{\varepsilon_0\varepsilon_{SAM}}\right) \quad (1)$$

Where *e* is elementary charge, *N* is the SAM packing density, μ_z is the SAM dipole component perpendicular to the dielectric

© 2014 WILEY-VCH Verlag GmbH & Co. KGaA, Weinheim

Table 1. Data from the z-component of the SAM dipole moment (μ_z), static water contact angle (SCA), the change in graphene/SAM/dielectric stack work function relative to the reference graphene/dielectric device ($\Delta\Phi_{Gr/SAM}$), the mean Dirac voltage (V_{Dirac}), electron mobility (μ_e), and hole mobility (μ_h) for graphene/SAM transistors with Au source and drain electrodes.

SAM	μ_z [D]	SCA [deg]	$\Delta\Phi_{Gr/SAM}$ [eV]	V_{Dirac} [V]	μ_e [$cm^2 V^{-1} s^{-1}$]	μ_h [$cm^2 V^{-1} s^{-1}$]
Ref[a)]	n/a[b)]	<10	n/a[b)]	−7.33 ± 0.78	802 ± 189	1611 ± 376
MeO	−2.02	63.9	−0.12 ± 0.02	−10.88 ± 1.48	856 ± 257	1115 ± 318
MeS	−1.49	68.1	0.03 ± 0.01	−5.76 ± 0.86	1327 ± 294	2053 ± 317
Ph	−0.74	60.5	−0.07 ± 0.01	−8.70 ± 2.73	665 ± 285	1164 ± 485
CF_3	1.92	75.3	0.19 ± 0.03	12.32 ± 3.91	774 ± 140	1441 ± 271
CN	3.88	57.3	0.29 ± 0.02	15.91 ± 3.85	693 ± 181	1225 ± 267

[a)]Ref represents device with no SAM treatment on dielectric surface, graphene only; [b)] Not applicable.

plane, ε_0 is the permittivity of free space, and ε_{SAM} is the relative permittivity of the SAM. From Equation 1, a linear relationship between the change in work function of the graphene/SAM stack and the SAM dipole moment is expected provided that the relative dielectric constant and packing density for each SAM is similar. This is a reasonable expectation given the similarity between each SAM molecule. Assuming a relative dielectric constant of 2.5, the packing density of each SAM is calculated to be approximately 5E13 molecules per square centimeter, which is near the expected theoretical value.[52]

It should be noted that the reference device with no SAM of graphene/dielectric was given a dipole magnitude of 0 D due to the additive nature of dipoles along the same direction.[53] Since the same base dielectric system is used across all characterized systems it is reasonable to assume that effect of the bare dielectric surface is uniform. An exception to the linear relationship between SAM dipole component and change in work function is the MeS SAM. It is hypothesized that the strong interaction between π-conjugated carbon and sulfur[54–56] results in a stronger interaction between the SAM and graphene upon device annealing. In addition, annealing may cause the MeS SAM to locally react with vacancy or edge defects within the graphene film which has been shown to induce hole doping.[57] Representative carbon 1s binding energy peaks can be seen in Figure 3b that show a shift towards lower binding energy (blue shift) as the p-type SAM character increases and higher binding energy (red shift) as the n-type SAM character increases which is in agreement with reported results.[23] These results also fall in line with the measured shift in work function, including MeS, which shows slight p-type character.

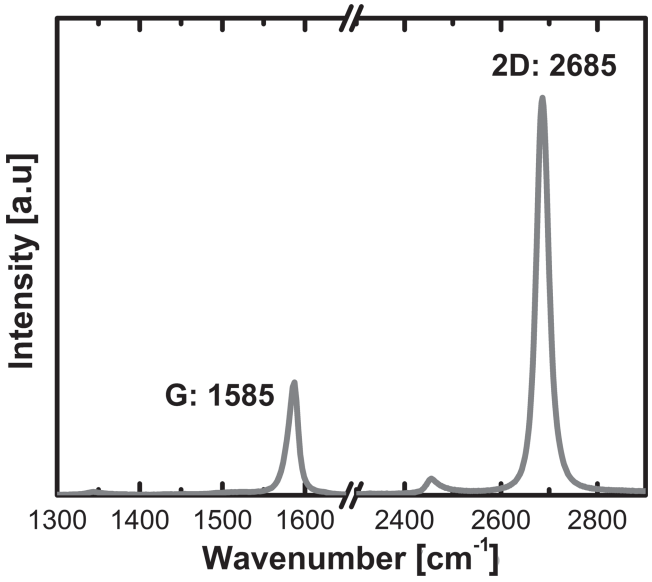

Figure 2. Representative Raman spectra of graphene on SAM signifying high quality graphene.

In order to further understand the effect of SAM dipoles on graphene, graphene transistors on SAM-modified AlO_x/300 nm SiO_2 were fabricated. Transistor channel width was 1000 µm while channel length varied between 12 µm and 100 µm. A schematic of the device structure and typical transfer curves of the graphene devices are shown in **Figure 4**a,b. The low hysteresis in these devices indicates an insignificant amount of adsorbed water and oxygen molecules that have recently been shown to be the origin of hysteresis in graphene via a redox reaction.[58] The average total resistance at the charge neutrality point is 5.5 kΩ, 4.4 kΩ, 6.6 kΩ, 4.3 kΩ, 6.6 kΩ, and 4.8 kΩ for CN, CF_3, Ph, MeS, MeO and the Ref device with no SAM treatment, respectively. This slight variation in resistance may be due to several factors such as differences in contact or sheet resistance from each individual SAM because of differing doping levels, charge impurities, or scattering sites. Several factors could affect contact resistance such as the thickness of the SAM molecule and its particular dipole. Secondly, the SAMs are shown later in this manuscript to influence the work function of graphene which may further influence contact resistance. The extrinsic field-effect mobility of graphene was extracted from the maximum slope near the charge neutrality point with the following equation:

$$\mu_{FET} = \frac{L_{ch}\left(\frac{dI_{ds}}{dV_{gs}}\right)}{W_{ch}C_{ox}V_{DS}} \quad (2)$$

where L_{ch} and W_{ch} is the channel length and width respectively, C_{ox} is the gate-oxide capacitance per area, and V_{DS} is the constant drain-source voltage.[59]

Averaged field-effect mobility can be seen in Table 1. Mobility values do not deviate significantly throughout all

© 2014 WILEY-VCH Verlag GmbH & Co. KGaA, Weinheim

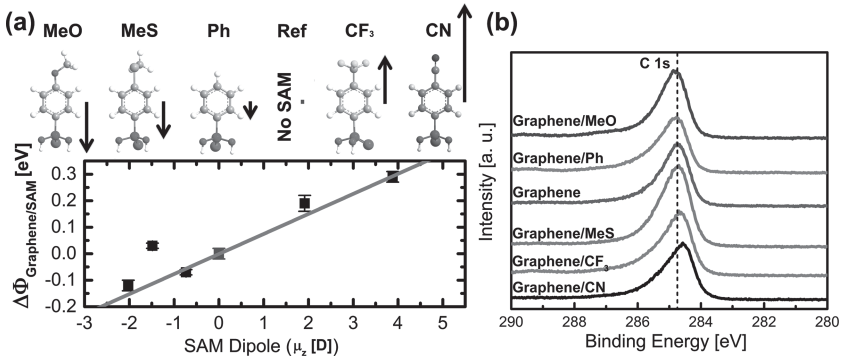

Figure 3. a) Visual representation of predicted z-component of SAM dipole (μ_z). Change in graphene/SAM work function as measured by XPS with respect to μ_z. The outlier of the linear fit is the MeS SAM which displays a strong interaction with graphene. b) C 1s binding energy peak for various graphene/SAMs used in this study. Direct correlation between peak position and SAM dipole is observed.

measured channel lengths. Although most of the graphene devices on SAM-treated dielectrics exhibited slightly lower mobilities than the reference device without SAM treatment (hole mobilities of 1200 $cm^2\ V^{-1}\ s^{-1}$ and 1600 $cm^2\ V^{-1}\ s^{-1}$, respectively), the MeS SAM treated devices very surprisingly exhibit significantly enhanced hole and electron mobility with values of 2053 $cm^2\ V^{-1}\ s^{-1}$ and 1327 $cm^2\ V^{-1}\ s^{-1}$, respectively. This enhancement may be due to the strong π-conjugated carbon and sulfur interaction between the SAM and graphene (as seen in XPS results) results in the transfer of graphene with less wrinkles and tears. Additionally, a general correlation between the total resistance and the extrinsic hole mobility is observed for SAM-treated devices with the lowest resistance having the highest mobility. This same correlation is not seen for electron mobility most likely due to the sensitivity of electrons to charge traps. This enhancement of mobility may indicate a reduction in contact resistance and remains an area to be further studied. Subsequently, thio-functionalized SAMs may prove to be a potential avenue to obtain high performance graphene transistors.

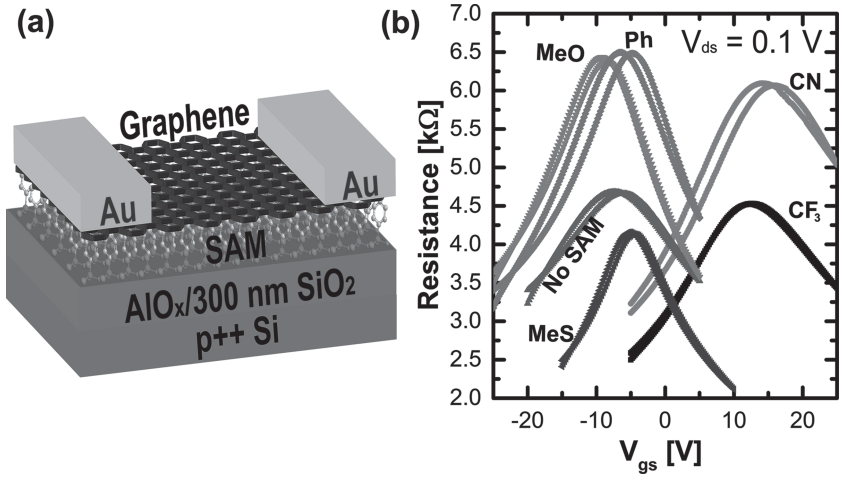

Figure 4. a) Schematic of graphene transistors fabricated and used in this study. b) Representative output curves (forward and backward sweep) of graphene transistors with various SAM-treated substrates.

The charge neutrality point (V_D) is defined as the conductivity minimum of the transfer curve.[60] V_D for each tested device was determined and averaged data were interrelated to the calculated SAM dipoles in Figure 3b. These data follow a general trend in which the SAM direction and magnitude is a baseline predictor for V_D. Based on the understanding of the electronic structure of graphene, it is possible to correlate the V_D shift to the change in Fermi energy as measured by XPS and discussed previously. Due to the linear band structure of graphene, the shift in Fermi energy induced by the SAM dipole can be described as follows:

$$\Delta E = \hbar v_F \sqrt{\pi n (V_{D2} - V_{D1})} \quad (3)$$

where n is the intrinsic carrier density per volt[61] with a typical value of approximately 7.2×10^{10} $cm^{-2}\ V^{-1}$, v_F is the Fermi velocity[62] previously reported as 1.1E6 m s^{-1}, and V_{D2} (V_{D1}) is the charge neutrality point of devices with (without) SAM treatment. Appropriately, it is expected that ΔE induced by the SAM should follow a linear relationship with the change in work function of the graphene/SAM devices previously measured via XPS. A linear fit is seen in **Figure 5**a with the exception for CN SAM.

In order to explain the similarity of V_D and thus ΔE for CF_3 and CN SAM treated dielectrics, we attribute this difference as the influence of doping from the metal electrodes. Previously, the results from DFT calculations have illustrated the doping of graphene on Cu with various metal contacts.[63,64] It was found that physisorbed metals such as Pt, Au, Cu, Ag, and Al can dope graphene to generate holes or electrons depending on the difference between the work function of metal and graphene, and the energy offset related to the separation distance between the metal and graphene. For example, if the separation distance between graphene and the metal is large (5 Å) the crossover from n-type to p-type doping occurs when the metal work function is equal to the work function of graphene. However, the equilibrium spacing for gold is expected to be 3.3 Å which results in a crossover from n-type to p-type doping when the metal is approximately 0.9 eV lower than that of graphene. It is thus predicted that CN and CF_3 SAMs cause the work function of graphene to become close enough to gold that the metal electrode changes from being a p-dopant to that of an n-dopant. This explains why V_D for CN is near that of CF_3 since increasing n-doping from the gold electrodes will result in a negative shift of charge neutrality point. The total change in ΔE is then related to the following equation:

$$\Delta E \approx \Delta\Phi_{graphene/SAM} + \Delta\Phi_{electrode/SAM} \quad (4)$$

It should be noted that the induced doping from metal electrode, $\Delta\Phi_{electrode/SAM}$, should

© 2014 WILEY-VCH Verlag GmbH & Co. KGaA, Weinheim

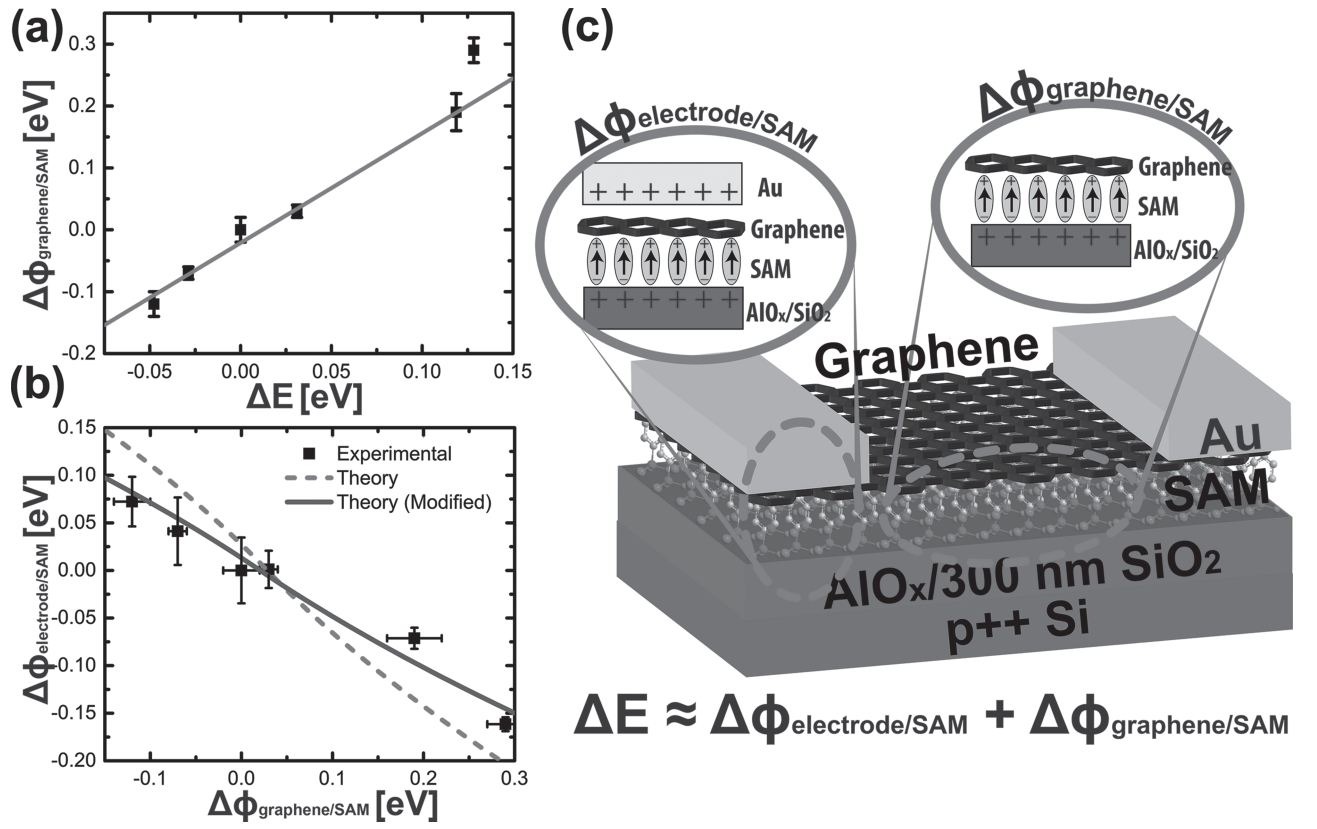

Figure 5. a) Shift in graphene/SAM work function (measured via XPS) with respect to the total energy shift (determined from FET charge neutrality position) and b) experimental, theoretical, and modified theoretical results comparing the influence of the contributions of each interface on the total energy shift. c) Schematic showing that both the electrode/graphene/SAM/dielectric interface and the graphene/SAM/dielectric interface must both be taken into account in order to predict the total shift in energy.

take into account the influence of the SAMs under graphene since the device structure employs an electrode stack of Au/graphene/SAM as seen previously in Figure 4. It is then possible to compare the experimentally determined value $\Delta\Phi_{electrode/SAM}$ with the expected theoretical value[65] shown in Figure 5b. While a slight deviation of measured and theoretical data occurs, a correction factor can be applied to compensate for this discrepancy,[66] which may be related to the interaction of the SAM dipole on the work function of the gold metal.

The original theoretical predictions assume that graphene on Cu has little to no influence on the properties of graphene. However, in this particular work, there is significant influence of the underlying SAM on the properties of graphene and it is reasonable to expect that due to the ultrathin nature of graphene, the dipole of SAM should have some contributions to the work function of the metal electrode except some screening effect due to graphene. Figure 5c shows an overall schematic of the influences of various interfaces on the properties of a graphene transistor with a SAM modified dielectric. It is important to consider all interfacial effects in order to reliably predict and control the properties of graphene transistors.

3. Conclusion

In summary, a clear relationship between SAM molecular dipole and graphene device performance was found to help predict the properties of graphene-based transistors. This is crucial for future applications and may enable predictable and controlled band-gap opening of bilayer graphene without the need for a dual gate architecture via self-assembled monolayers.[67,68] We have presented direct experimental evidence that shows systematic and precise control of the charge neutrality point of graphene/SAM transistors is possible by carefully tuning the SAM and metal contact without having a negative impact on device performance.

4. Experimental Section

Device Fabrication and Testing: CVD monolayer graphene was grown on copper foil at 990 °C in flowing methane and hydrogen gas at 0.002 and 0.035 slm respectively. Standard poly(methyl methacrylate) (PMMA) was then spin coated on top of graphene as a support layer. The underlying copper foil was then etched away using aqueous ammonium persulfate leaving only graphene supported by PMMA floating in the solution. Graphene/PMMA was then transferred to several different baths of deionized water in order to clean the membrane from etchant and metal impurities.

All SAMs utilized the same assembly process in which heavily p-doped Si/300 nm SiO_2 substrates were cleaned with piranha (30% aqueous hydrogen peroxide and 12 M sulfuric acid in a 1:4 volume ratio) followed by sonication in RCA (ammonium hydroxide, 30% aq. hydrogen peroxide, and deionized water in a 1:1:5 volume ratio), and then extensive rinsing in deionized water. Substrates were then plasma cleaned for 30 min resulting in a 2–3 nm layer of AlO_x as described previously.[33]

© 2014 WILEY-VCH Verlag GmbH & Co. KGaA, Weinheim

Phosphonic acid compounds for SAMs were dissolved in a mixed solvent of tetrahydrofuron (THF) and ethanol (EtOH) (1:1 vol ratio, 0.1 mM concentration), sonicated until complete dissolution, and then filtered with a 0.2 μm PTFE filter. Cleaned substrates were then immersed in the filtered solution and assembly was allowed to occur at room temperature over the course of 48 h. Upon the completion of assembly, the formed SAMs on substrates were annealed at 120 °C for 15 min followed by cleaning via sonication in dimethylformamide, THF, and EtOH in order to remove any residual aggregates.

PMMA supported graphene was then transferred onto assembled SAM substrates and allowed to dry over the course of 24 h. Afterwards PMMA on top the graphene/SAM/substrates was removed via rinsing in hot (≈60 °C) acetone over several hours followed by an isopropyl alcohol rinse.

Shadow masks were then used to fabricate 40 nm thick Au source and drain electrodes using standard thermal evaporation under high vacuum (10^{-7} Torr). Devices were subsequently annealed at 200 °C under nitrogen and characterized immediately using an Agilent 4155B semiconductor parameter analyzer. Reported electrical characteristics are an average of more than 15 devices with channel lengths varying between 12, 20, 30, 50, 80, and 100 μm. No significant deviation in performance or charge neutrality point was seen with respect to transistor channel length.

AFM, Contact Angle Goniometry, and Raman Spectroscopy: Digital Instruments Multimode Nanoscope IIIa scanning probe microscope (Veeco Instruments, Plainview, NY) was used in AFM tapping mode. Aqueous static contact angle values were taken with a VCA Optima Surface Analysis System (Adv. Surface Technology Products, Billerica, MA) and are an average of five measurements with a standard deviation of less than ±3°. An inVia Raman Microscope (Renishaw, Cook, IL) with 514 nm laser was used to determine the quality of graphene on dielectric surface via the characteristic phonon peaks of graphene and is averaged data of more than 10 scans sweep from 3000 to 1000 cm^{-1} and a resolution of 2.5 cm^{-1}.

XPS Characterization: XPS measurements were performed under ultrahigh vacuum (5×10^{-10} Torr) with a PHI VersaProbe X-ray photoelectron spectrometer (ULVAC-PHI, Kanagawa, Japan) using a monochromatic focused Al-Kα X-ray source ($h\nu$ = 1486.70 eV) and hemispherical analyzer. In order to achieve a high resolution spectrum for characterization of the C 1s peak a pass energy of 23.5 eV was used. Work function measurements are an average of approximately 14 positions on a given substrate and characterized with a pass energy of 2.95 eV. The large number of data points were necessary to ensure consistency due to the fact that the samples were exposed to atmosphere before measurement. It is possible that even though exposure was brief (only a few seconds during sample transfer) adsorbed species may partially screen the dipole field resulting in a lower work function shift versus dipole strength while still remaining linear.

Acknowledgements

The authors thank C. M. Jäger for his assistance with the density functional theory calculations. The authors thank F. S. Ohuchi and M. A. Olmstead for use of their XPS system. This work is supported by AFOSR. A.K.-Y.J. acknowledges the Boeing-Johnson Professorship for its support.

Received: November 24, 2013
Revised: December 26, 2013
Published online: March 5, 2014

[1] A. H. Castro Neto, N. M. R. Peres, K. S. Novoselov, A. K. Geim, *Rev. Mod. Phys.* **2009**, *81*, 109.
[2] K. S. Novoselov, A. K. Geim, S. V. Morozov, D. Jiang, M. I. Katsnelson, I. V. Grigorieva, S. V. Dubonos, A. A. Firsov, *Nature* **2005**, *438*, 197.
[3] P. Wallace, *Phys. Rev.* **1947**, *71*, 622.
[4] K. I. Bolotin, K. J. Sikes, Z. Jiang, M. Klima, G. Fudenberg, J. Hone, P. Kim, H. L. Stormer, *Solid State Commun.* **2008**, *146*, 351.
[5] S. V. Morozov, K. S. Novoselov, M. I. Katsnelson, F. Schedin, D. C. Elias, J. A. Jaszczak, A. K. Geim, *Phys. Rev. Lett.* **2008**, *100*, 016602.
[6] T. O. Wehling, M. I. Katsnelson, A. I. Lichtenstein, *Chem. Phys. Lett.* **2009**, *476*, 125.
[7] X. Liang, B. A. Sperling, I. Calizo, G. Cheng, C. A. Hacker, Q. Zhang, Y. Obeng, K. Yan, H. Peng, Q. Li, X. Zhu, H. Yuan, A. R. Hight Walker, Z. Liu, L.-M. Peng, C. A. Richter, *ACS Nano* **2011**, *5*, 9144.
[8] A. S. Mayorov, R. V. Gorbachev, S. V. Morozov, L. Britnell, R. Jalil, L. A. Ponomarenko, P. Blake, K. S. Novoselov, K. Watanabe, T. Taniguchi, A. K. Geim, *Nano Lett.* **2011**, *11*, 2396.
[9] R. A. Nistor, M. A. Kuroda, A. A. Maarouf, G. J. Martyna, *Phys. Rev. B* **2012**, *86*, 041409.
[10] H. Liu, Y. Liu, D. Zhu, *J. Mater. Chem.* **2011**, *21*, 3335.
[11] K. C. Kwon, K. S. Choi, S. Y. Kim, *Adv. Funct. Mater.* **2012**, *22*, 4724.
[12] P. Wei, N. Liu, H. R. Lee, E. Adijanto, L. Ci, B. D. Naab, J. Q. Zhong, J. Park, W. Chen, Y. Cui, Z. Bao, *Nano Lett.* **2013**, *13*, 1890.
[13] H. H. Kim, J. W. Yang, S. B. Jo, B. Kang, S. K. Lee, H. Bong, G. Lee, K. S. Kim, K. Cho, *ACS Nano* **2013**, *7*, 1155.
[14] D. Wei, Y. Liu, Y. Wang, H. Zhang, L. Huang, G. Yu, *Nano Lett.* **2009**, *9*, 1752.
[15] Y. Xue, B. Wu, L. Jiang, Y. Guo, L. Huang, J. Chen, J. Tan, D. Geng, B. Luo, W. Hu, G. Yu, Y. Liu, *J. Am. Chem. Soc.* **2012**, *134*, 11060.
[16] Y.-B. Tang, L.-C. Yin, Y. Yang, X.-H. Bo, Y.-L. Cao, H.-E. Wang, W.-J. Zhang, I. Bello, S.-T. Lee, H.-M. Cheng, C.-S. Lee, *ACS Nano* **2012**, *6*, 1970.
[17] Y.-J. Yu, Y. Zhao, S. Ryu, L. E. Brus, K. S. Kim, P. Kim, *Nano Lett.* **2009**, *9*, 3430.
[18] Y. Shi, X. Dong, P. Chen, J. Wang, L.-J. Li, *Phys. Rev. B* **2009**, *79*, 115402.
[19] G. Giovannetti, P. A. Khomyakov, G. Brocks, V. M. Karpan, J. van den Brink, P. J. Kelly, *Phys. Rev. Lett.* **2008**, *101*, 026803.
[20] A. Varykhalov, M. R. Scholz, T. K. Kim, O. Rader, *Phys. Rev. B* **2010**, *82*, 121101.
[21] K. Yokota, K. Takai, T. Enoki, *Nano Lett.* **2011**, *11*, 3669.
[22] Z. Yan, Z. Sun, W. Lu, J. Yao, Y. Zhu, J. M. Tour, *ACS Nano* **2011**, *5*, 1535.
[23] J. Park, W. H. Lee, S. Huh, S. H. Sim, S. B. Kim, K. Cho, B. H. Hong, K. S. Kim, *J. Phys. Chem. Lett.* **2011**, *2*, 841.
[24] R. Wang, S. Wang, D. Zhang, Z. Li, Y. Fang, X. Qiu, *ACS Nano* **2010**, *5*, 408.
[25] B. de Boer, A. Hadipour, M. M. Mandoc, T. van Woudenbergh, P. W. M. Blom, *Adv. Mater.* **2005**, *17*, 621.
[26] J.-P. Hong, A.-Y. Park, S. Lee, J. Kang, N. Shin, D. Y. Yoon, *Appl. Phys. Lett.* **2008**, *92*, 143311.
[27] L. L. Chua, J. Zaumseil, J. F. Chang, E. C. Ou, P. K. Ho, H. Sirringhaus, R. H. Friend, *Nature* **2005**, *434*, 194.
[28] J. Youn, G. R. Dholakia, H. Huang, J. W. Hennek, A. Facchetti, T. J. Marks, *Adv. Funct. Mater.* **2012**, *22*, 1856.
[29] X. Y. Cheng, Y. Y. Noh, J. P. Wang, M. Tello, J. Frisch, R. P. Blum, A. Vollmer, J. P. Rabe, N. Koch, H. Sirringhaus, *Adv. Funct. Mater.* **2009**, *19*, 2407.
[30] U. Zschieschang, F. Ante, M. Schlorholz, M. Schmidt, K. Kern, H. Klauk, *Adv. Mater.* **2010**, *22*, 4489.
[31] U. Kraft, U. Zschieschang, F. Ante, D. Kälblein, C. Kamella, K. Amsharov, M. Jansen, K. Kern, E. Weber, H. Klauk, *J. Mater. Chem.* **2010**, *20*, 6416.
[32] A. Jedaa, M. Salinas, C. M. Jäger, T. Clark, A. Ebel, A. Hirsch, M. Halik, *Appl. Phys. Lett.* **2012**, *100*, 063302.
[33] O. Acton, D. Hutchins, L. Arnadottir, T. Weidner, N. Cernetic, G. G. Ting, T. W. Kim, D. G. Castner, H. Ma, A. K. Jen, *Adv. Mater.* **2011**, *23*, 1899.

© 2014 WILEY-VCH Verlag GmbH & Co. KGaA, Weinheim

[34] J. McElwee, R. Helmy, A. Y. Fadeev, *J. Colloid Interface Sci.* **2005**, *285*, 551.
[35] E. L. Hanson, J. Schwartz, B. Nickel, N. Koch, M. F. Danisman, *J. Am. Chem. Soc.* **2003**, *125*, 16074.
[36] P. H. Mutin, G. Guerrero, A. Vioux, *J. Mater. Chem.* **2005**, *15*, 3761.
[37] M. Salinas, C. M. Jäger, A. Y. Amin, P. O. Dral, T. Meyer-Friedrichsen, A. Hirsch, T. Clark, M. Halik, *J. Am. Chem. Soc.* **2012**, *134*, 12648.
[38] P. Hohenberg, *Phys. Rev.* **1964**, *136*, B864.
[39] W. Kohn, L. J. Sham, *Phys. Rev.* **1965**, *140*, A1133.
[40] M. J. Frisch, G. W. Trucks, H. B. Schlegel, G. E. Scuseria, M. A. Robb, J. R. Cheeseman, G. Scalmani, V. Barone, B. Mennucci, G. A. Petersson, H. Nakatsuji, M. Caricato, X. Li, H. P. Hratchian, A. F. Izmaylov, J. Bloino, G. Zheng, J. L. Sonnenberg, M. Hada, M. Ehara, K. Toyota, R. Fukuda, J. Hasegawa, M. Ishida, T. Nakajima, Y. Honda, O. Kitao, H. Nakai, T. Vreven, J. J. A. Montgomery, J. E. Peralta, F. Ogliaro, M. Bearpark, J. J. Heyd, E. Brothers, K. N. Kudin, V. N. Staroverov, R. Kobayashi, J. Normand, K. Raghavachari, A. Rendell, J. C. Burant, S. S. Iyengar, J. Tomasi, M. Cossi, N. Rega, J. M. Millam, M. Klene, J. E. Knox, J. B. Cross, V. Bakken, C. Adamo, J. Jaramillo, R. Gomperts, R. E. Stratmann, O. Yazyev, A. J. Austin, R. Cammi, C. Pomelli, J. W. Ochterski, R. L. Martin, K. Morokuma, V. G. Zakrzewski, G. A. Voth, P. Salvador, J. J. Dannenberg, S. Dapprich, A. D. Daniels, Ö. Farkas, J. B. Foresman, J. V. Ortiz, J. Cioslowski, D. J. Fox, *Gaussian 09, Revision A.02,* Gaussian, Inc. Wallingford CT **2009**.
[41] J. P. Perdew, K. Burke, M. Ernzerhof, *Phys. Rev. Lett.* **1996**, *77*, 3865.
[42] A. Schafer, H. Horn, R. Ahlrichs, *J. Chem. Phys.* **1992**, *97*, 2571.
[43] K. Eichkorn, O. Treutler, H. Öhm, M. Häser, R. Ahlrichs, *Chem. Phys. Lett.* **1995**, *242*, 652.
[44] R. J. Nemanich, S. A. Solin, *Phys. Rev. B* **1979**, *20*, 392.
[45] F. Tuinstra, J. L. Koenig, *J. Chem. Phys.* **1970**, *53*, 1126.
[46] L. Cançado, A. Reina, J. Kong, M. Dresselhaus, *Phys. Rev. B* **2008**, *77*, 245408.
[47] A. C. Ferrari, J. C. Meyer, V. Scardaci, C. Casiraghi, M. Lazzeri, F. Mauri, S. Piscanec, D. Jiang, K. S. Novoselov, S. Roth, A. K. Geim, *Phys. Rev. Lett.* **2006**, *97*, 187401.
[48] R. Schlaf, H. Murata, Z. H. Kafafi, *J. Electron. Spectrosc. Relat. Phenom.* **2001**, *120*, 149.
[49] S. Bae, H. Kim, Y. Lee, X. Xu, J. S. Park, Y. Zheng, J. Balakrishnan, T. Lei, H. R. Kim, Y. I. Song, Y. J. Kim, K. S. Kim, B. Ozyilmaz, J. H. Ahn, B. H. Hong, S. Iijima, *Nat. Nanotechnol.* **2010**, *5*, 574.
[50] S. E. Koh, K. D. McDonald, D. H. Holt, C. S. Dulcey, J. A. Chaney, P. E. Pehrsson, *Langmuir* **2006**, *22*, 6249.
[51] L. Kronik, Y. Shapira, *Surf. Sci. Rep.* **1999**, *37*, 1.
[52] M. Gliboff, L. Sang, K. M. Knesting, M. C. Schalnat, A. Mudalige, E. L. Ratcliff, H. Li, A. K. Sigdel, A. J. Giordano, J. J. Berry, D. Nordlund, G. T. Seidler, J.-L. Brédas, S. R. Marder, J. E. Pemberton, D. S. Ginger, *Langmuir* **2013**, *29*, 2166.
[53] P. C. Rusu, G. Brocks, *J. Phys. Chem. B* **2006**, *110*, 22628.
[54] X. Ji, K. T. Lee, L. F. Nazar, *Nat. Mater.* **2009**, *8*, 500.
[55] B. Zhang, X. Qin, G. R. Li, X. P. Gao, *Energy Environ. Sci.* **2010**, *3*, 1531.
[56] Y. Yang, M. T. McDowell, A. Jackson, J. J. Cha, S. S. Hong, Y. Cui, *Nano Lett.* **2010**, *10*, 1486.
[57] G. Hui, L. Zheng, S. Li, G. Wenhua, G. Wei, C. Lijie, R. Amrita, Q. Weijin, V. Robert, M. A. Pulickel, *Nanotechnology* **2012**, *23*, 275605.
[58] H. Xu, Y. Chen, J. Zhang, H. Zhang, *Small* **2012**, *8*, 2833.
[59] F. Schwierz, *Nat. Nanotechnol.* **2010**, *5*, 487.
[60] P. Avouris, *Nano Lett.* **2010**, *10*, 4285.
[61] S. Pisana, M. Lazzeri, C. Casiraghi, K. S. Novoselov, A. K. Geim, A. C. Ferrari, F. Mauri, *Nat. Mater.* **2007**, *6*, 198.
[62] Y. Zhang, V. W. Brar, F. Wang, C. Girit, Y. Yayon, M. Panlasigui, A. Zettl, M. F. Crommie, *Nat. Phys.* **2008**, *4*, 627.
[63] P. A. Khomyakov, G. Giovannetti, P. C. Rusu, G. Brocks, J. van den Brink, P. J. Kelly, *Phys. Rev. B* **2009**, *79*, 195425.
[64] M. Vanin, J. J. Mortensen, A. K. Kelkkanen, J. M. Garcia-Lastra, K. S. Thygesen, K. W. Jacobsen, *Phys. Rev. B* **2010**, *81*, 081408.
[65] The Fermi level shift equation from reference 63 to determine the influence of Au metal doping on graphene was used: $\Delta\Phi_{\text{Electrode}}(d) = \pm\frac{\sqrt{1+2\alpha D_0(d-d_0)|W_M - W_G - \Delta_c(d)|}-1}{\alpha D_0(d-D_0)}$ and $\Delta_c(d) = e^{-\gamma d}\left(a_0 + a_1 d + a_2 d^2\right)$ The parameter d represents the separation distance between the metal electrode and graphene with an equilibrium value determined to be 3.3 Å. The work function of Au (W_M) was set as 5.25 eV, while W_G represented the measured value of the graphene/SAM work function. Other parameters are standard parameters related to the graphene unit cell and are detailed further in reference 63.
[66] In order to compensate for interaction/shielding effect between the underlying SAMs on graphene and the metal electrode work function, it was assumed that the effective dipole was reduced and a correction factor was applied. For this factor, W_G from the equation in reference 65 was changed to $W_{G0} + b \times \Delta\Phi_{SAM}$. Where $\Delta\Phi_{SAM}$ is the deviation from the untreated work function of graphene caused by the SAM and b is the correction factor equal to 0.679. W_{G0} is the untreated work function of graphene measured to be 4.31 eV.
[67] J. Park, S. B. Jo, Y.-J. Yu, Y. Kim, J. W. Yang, W. H. Lee, H. H. Kim, B. H. Hong, P. Kim, K. Cho, K. S. Kim, *Adv. Mater.* **2012**, *24*, 407.
[68] J. W. Yang, G. Lee, J. S. Kim, K. S. Kim, *J. Phys. Chem. Lett.* **2011**, *2*, 2577.

© 2014 WILEY-VCH Verlag GmbH & Co. KGaA, Weinheim